BaF$_2$ for microlithography applications: Modeling, simulation and optimization of the crystal growth process$^{☆}$

Rainer Backofen[a], Angel Ribalta[a], Axel Voigt[a,*], Dirk Wulff-Molder[b]

[a]*Crystal Growth Group, Research Center Caesar, Ludwig-Erhard-Allee 2, 53175 Bonn, Germany*
[b]*Korth Kristalle GmbH, Am Jägersberg 3, 24161 Altenholz (Kiel), Germany*

Abstract

Optimization is the ultimate goal of numerical modeling of crystal growth processes. We present the most important physical phenomena to establish a numerical process model for an industrial vertical gradient freeze (VGF) process of barium fluoride (BaF$_2$). After reviewing the governing equations we describe an adaptive finite element approach for a phase change problem with internal radiation. We describe an interface to a commercial software package for industrial crystal growth processes to define a numerical process model in a highly automatized way. In this way we can apply an external optimization algorithm to our process model. We use a modified quasi-Newton method to propose an improvement of an industrial VGF growth process of BaF$_2$.
© 2006 Elsevier B.V. All rights reserved.

1. Introduction

In order to decrease size of integrated circuits, lithography has to be extended to smaller wavelength. Currently industry makes a lot of efforts to implement 157-nm lithography to achieve sub 100-nm scale technology [6]. For this wavelength new materials are needed for lenses. Lenses of fluoride crystals (BaF$_2$, CaF$_2$) show the needed optical properties. Due to optical and mechanical properties CaF$_2$ is thought to be the key material for lenses. But in order to overcome the internal birefringence of CaF$_2$ systems with lenses of additional material are needed [6,7]. So there is a demand of high quality BaF$_2$ crystals.

An well established method in crystal growth industry to produce high quality optical and semiconductor crystal is the vertical gradient freeze (VGF) technique [2,16,14]. In a crucible an axial temperature gradient is established, see Fig. 1. The temperature is then shifted slowly to solidify the material from a seed at the bottom. This is done either by moving the crucible downwards from a hot to a cold heater or by shifting the thermal field in the furnace by changing the power of the heaters in time. A VGF growth process may be done in a highly homogeneous temperature field
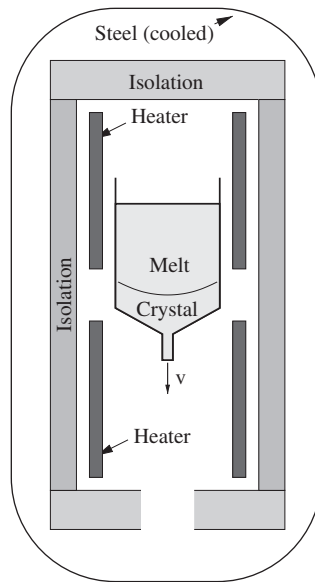
Fig. 1. VGF (Bridgmann) process.

with small axial and radial gradients in the crystal. This leads to small thermoelastic stress, a main source of crystal defects [12].

Numerical modeling of the growth process has already proved their applicability to understand and improve crystal growth [15,16]. Although the main interest in modeling is the temperature in the crystal, a complete numerical model of the process has to account for a lot of physical phenomena. In general heat transport by conduction, convection and radiation, mass transport and the free phase boundary has to be modeled in a complex geometry. There are quite a few commercial software packages, which are used in industry to model such growth processes (Fidap [10], CrysVUn [9], STHAMAS [9], CFD-ACE [8]). They provide a short developing cycle from a CAD-drawing to a numerical model of the process and are robust in solving the underlying set of nonlinear PDEs.

Quantitative process modeling and optimization suffers from a lot of uncertainties and constraints in the set-up of the numerical process model. On the one hand the properties of the used materials may be badly specified. The material properties may not be known at the requested temperatures or atmosphere. Additionally the properties may change due to aging and reactive atmosphere. On the other hand the physical models often use some approximation. To overcome this problem the uncertain material parameters have to be identified from experimental data for each individual process or furnace. This already sets the first stage of an optimization loop: find appropriate model parameters in a process model which numerically describe the industrial process within a given tolerance. After this loop and a validation of the derived process model a second optimization loop follows which optimizes the process parameters to improve the industrial process, see Fig. 2.

These two steps, adapting and optimization of the numerical model, are just the inner part of a developing cycle to understand and improve a process. New experiments lead to additional adaption and further optimization.

In this paper we have to goals. On the one hand we will improve the modeling of crystal growth and on the other hand we are concerned with optimization of crystal growth processes. So the paper separates in two parts.

In Section 2 we summarize the modeling of the most important physical phenomena in order to develop a numerical model of crystal growth. We also motivate some typical approximations and simplifications often used in crystal growth modeling. A numerical algorithm for a higher order diffusive approximation for internal radiation is presented.

In Section 3 the difficulties and constraints of defining a process model adequate for process optimization is discussed and an interface between a commercial software package and an optimization method is described.

In Section 4 a numerical process model is adapted to an industrial crystal growth process of BaF_2. The adapted model is used to improve the process parameter and an improved growth process is proposed.
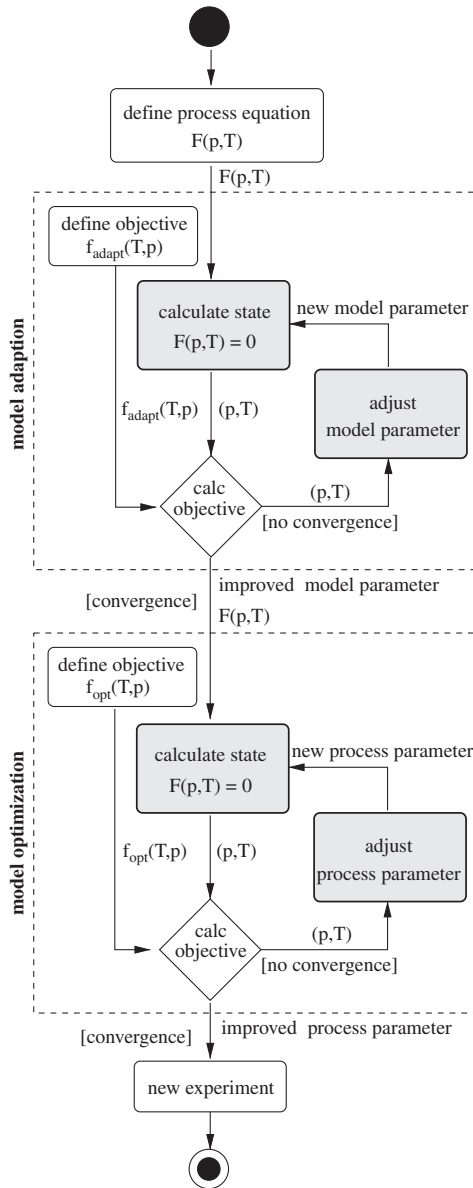
Fig. 2. Optimization framework.

2. Modeling of crystal growth processes

The governing equation to describe heat transport in crystal growth is the nonlinear heat equation

$$\rho c_p \left(\frac{\partial}{\partial t} T + \vec{u} \cdot \nabla T \right) = \nabla \cdot \vec{i}_q + Q, \tag{1}$$

for temperature T. Here ρ is density, c_p is specific heat capacity, $\vec{u}$ is velocity, $\vec{i}_q$ is heat flux and Q is heat source. This equations is valid in all parts of the system and has to be supplemented by governing equations for $\vec{u}$, $\vec{i}_q$ and Q as well as appropriate initial and boundary conditions. At the crystal–melt interface boundary conditions for the temperature

are given by

$$\vec{i}_{q,\text{crystal}} \cdot \vec{n} - \vec{i}_{q,\text{melt}} \cdot \vec{n} = \rho_{c_0} L(\vec{u}_{\text{crystal}} - \vec{u}_{\text{interface}}) \cdot \vec{n}, \tag{2}$$

with L the latent heat, $\vec{n}$ the unit normal and

$$T = T_{\text{eq}} - \underbrace{\frac{\sigma_{\text{interface}} H}{\rho_{c_0} L}}_{\text{curvature undercooling}} - \alpha \underbrace{\frac{\sigma_{\text{interface}}(\vec{u}_{\text{crystal}} - \vec{u}_{\text{interface}}) \cdot \vec{n}}{\rho_{c_0} L}}_{\text{kinetic undercooling}},$$

with T_{eq} the equilibrium temperature, $\sigma_{\text{interface}}$ the surface free energy, H curvature and α a kinetic coefficient.

2.1. Heat source

The heat source, Q, corresponds to resistance or induction heating or chemical reactions and will be assumed as a given quantity.

2.2. Melt convection

The density variations in the melt are very small and can therefore be treated as constant. This leads to the incompressible Navier–Stokes equations

$$\nabla \cdot \vec{u} = 0 \tag{3}$$

and

$$\rho \left(\frac{\partial}{\partial t} \vec{u} + (\vec{u} \cdot \nabla) \vec{u} \right) = \vec{f} - \nabla p + \mu \Delta \vec{u}, \tag{4}$$

with p the pressure, μ the viscosity and $\vec{f}$ a forcing term. On the other hand density variations due to variations of temperature induce convection and should not be treated as constant in the calculation of the body forces induced by thermal buoyancy. The assumption of a linear dependence of the melt density on temperature leads to the Boussinesq approximation:

$$\vec{f} = \rho_0 (1 + \beta_T (T - T_0)) \vec{g}, \tag{5}$$

with β_T the thermal expansion coefficients, T_0 a reference values for temperature, ρ_0 a reference density calculated from the ideal gas law at the reference temperature and $\vec{g}$ the gravitational acceleration. In all other terms the density ρ is treated as constant. Boundary conditions for the velocity are given by no-slip assumptions. We assume that the melt perfectly adheres to the crucible wall and specify

$$\vec{u} = \vec{u}_{\text{crucible}}. \tag{6}$$

At the solid–liquid interface the crystal is assumed to behave like a rigid body. The no-slip conditions as well as mass-conservation read therefore

$$\rho_{0,\text{melt}} (\vec{u} - \vec{u}_{\text{interface}}) \cdot \vec{n} = \rho_{0,\text{crystal}} (\vec{u}_{\text{crystal}} - \vec{u}_{\text{interface}}) \cdot \vec{n}, \tag{7}$$

$$\vec{u} \cdot \vec{t} = \vec{u}_{\text{crystal}} \cdot \vec{t}, \tag{8}$$

where $\vec{t}$ is a tangential vector on the interface.

2.3. Heat conduction

The heat flux $\vec{i}_q$ is composed of a flux due to heat conduction $\vec{i}_{q_c}$ and a flux due heat radiation $\vec{i}_{q_r}$. Fourier's law relates the heat flux due to conduction to the temperature gradient by

$$\vec{i}_{q_c} = -k \nabla T, \tag{9}$$

with k the heat conduction coefficient.

2.4. Heat radiation

The radiative flux $\vec{i}_{q_r}$ can be computed using the radiative intensity I, which is for a given frequency v the amount of energy that, during a given time interval, passes through a unit area perpendicular to the direction ω of the rays per unit solid angle. Inside a medium, I is related to $\vec{i}_{q_r}$ by

$$\vec{i}_{q_r}(v) = \int_{S^2} I(\omega, v)\omega \, \mathrm{d}\omega. \tag{10}$$

For a black surface the emitted intensity for a given temperature T is according to Planck's law given by

$$I_B(v) = \frac{2hv^3 n^2}{c_0^2} \frac{1}{\mathrm{e}^{hv/k_B T} - 1}, \tag{11}$$

with h Planck's constant, k_B Boltzmann's constant, n refraction index and c_0 speed of light. The total emitted intensity can be computed by integrating over v

$$I_B = \frac{1}{\pi} n^2 \sigma T^4, \tag{12}$$

with σ the Stefan–Boltzmann constant. The transport equation for radiation in a medium can now be derived from a balance equation for the ray where attenuation by absorption, emission and scattering is taken into account. The amount of absorption is proportional to the magnitude of the incident radiation and can be written as $-\kappa I$, with κ the absorption coefficient. Assuming local thermodynamic equilibrium, the coefficients of absorption and emission are the same and the amount of emission is again proportional to the magnitude of the incident radiation, κI_B. Besides absorption and emission the intensity I may also be influenced by scattering. The intensity is weakened by scattering away from the direction of incidence. Again the amount is proportional to the magnitude $-\sigma_s I$, with σ_s the scattering coefficient. Moreover, incident rays from different directions ω' may be scattered in the direction ω, thereby increasing the intensity. The fraction $\Phi(\omega', \omega)/4\pi$ of the scattered amount $\sigma_s I(\omega')$ from a direction ω' is redirected into the direction ω. The function $\Phi(\omega', \omega)$ is the so-called scattering phase function. In order to describe the increase of the intensity due to this phenomenon contributions from all incident directions have to be added. Under the assumption that changes of the intensity are instantaneous, the equation of transport for radiation for each frequency v can now be written as

$$\omega \cdot \nabla I = -\kappa I + \kappa I_B - \sigma_s I + \frac{\sigma_s}{4\pi} \int_{S^2} I(\omega')\Phi(\omega', \omega) \, \mathrm{d}\omega'. \tag{13}$$

The divergence of $\vec{i}_{q_r}$ can be written using Eq. (13)

$$\begin{aligned}
\nabla \cdot \vec{i}_{q_r} &= \int_{S^2} \omega \cdot \nabla I(\omega) \, \mathrm{d}\omega \\
&= -(\kappa + \sigma_s) \int_{S^2} I(\omega) \, \mathrm{d}\omega + \kappa \int_{S^2} I_B \, \mathrm{d}\omega + \frac{\sigma_s}{4\pi} \int_{S^2} I(\omega') \int_{S^2} \Phi(\omega', \omega) \, \mathrm{d}\omega \, \mathrm{d}\omega' \\
&= \kappa \int_{S^2} I_B - I(\omega) \, \mathrm{d}\omega,
\end{aligned}$$

where the identity $\int_{S^2} \Phi(\omega', \omega) \, \mathrm{d}\omega = 4\pi$ is used. By integrating over v Eq. (1) can now be written as

$$\rho c_p \left(\frac{\partial}{\partial t} T + \vec{u} \cdot \nabla T \right) = \nabla \cdot (k\nabla T) - \int_0^\infty \kappa \int_{S^2} I_B - I(\omega, v) \, \mathrm{d}\omega \, \mathrm{d}v + Q \tag{14}$$

and has to be supplemented by the transport equation for the intensity of the radiative field (13). The radiative field not only depend on position and time as the other quantities considered do, but also on the direction ω in space and the frequency v. Therefore, the computational complexity of solving the transport equation is very high, and only approximations will be considered in the following sections.

2.4.1. Internal radiation

Scattering is usually neglected in the transport equation for the radiative field. Assuming the scattering coefficient σ_s to be zero a diffusive approximation known as SP_N approximation can be derived [13]. The optically thick regime, where the absorption coefficient κ is large, can be considered in a diffusion-like manner. To obtain a diffusion scaling, the parameter $\varepsilon = 1/\kappa_{\text{ref}}x_{\text{ref}}$ and an appropriate rescaling is introduced, leading to

$$\varepsilon\omega \cdot \nabla I = \kappa I + \kappa I_{\text{B}}, \tag{15}$$

or

$$\left(1 + \frac{\varepsilon}{\kappa}\omega \cdot \nabla\right) I = I_{\text{B}}. \tag{16}$$

Applying a Neumann series to formally invert the transport operator lead to

$$I = \left(1 + \frac{\varepsilon}{\kappa}\omega \cdot \nabla\right)^{-1} I_{\text{B}} \tag{17}$$

$$= \left(1 - \frac{\varepsilon}{\kappa}\omega \cdot \nabla + \frac{\varepsilon^2}{\kappa^2}(\omega \cdot \nabla)^2 - \frac{\varepsilon^3}{\kappa^3}(\omega \cdot \nabla)^3 + \frac{\varepsilon^4}{\kappa^4}(\omega \cdot \nabla)^4\right) I_{\text{B}}. \tag{18}$$

Now integrating over ω, using $\int_{S^2}(\omega \cdot \nabla)^n \, d\omega = (1 + (-1)^n)(2\pi/(n+1))\nabla^n$ and defining

$$\phi = \int_{S^2} I \, d\omega \tag{19}$$

leads by again formally applying a Neumann series to

$$4\pi I_{\text{B}} = \left(1 - \frac{\varepsilon^2}{3\kappa^2}\nabla^2 - \frac{4\varepsilon^4}{45\kappa^4}\nabla^4 - \frac{44\varepsilon^6}{945\kappa^6}\nabla^6\right)\phi + \text{O}(\varepsilon^8). \tag{20}$$

When terms of $\text{O}(\varepsilon^2)$, $\text{O}(\varepsilon^4)$, $\text{O}(\varepsilon^6)$ or $\text{O}(\varepsilon^8)$ are discarded the SP_0, SP_1, SP_2 or SP_3 approximations are obtained. Even if this formal derivation is obtained for constant parameters κ the resulting equations are assumed to be valid also for nonconstant parameters:

SP_0 *approximation*:

$$\phi = 4\pi I_{\text{B}},$$

$$\rho c_p \left(\frac{\partial}{\partial t}T + \vec{u} \cdot \nabla T\right) = \nabla \cdot (k\nabla T) + \int_0^\infty \nabla \cdot \frac{1}{3\kappa}\nabla\phi \, dv + Q,$$

which reduced to an equation for the temperature T alone, and is the conventional Rosseland approximation.

$$\rho c_p \left(\frac{\partial}{\partial t}T + \vec{u} \cdot \nabla T\right) = \nabla \cdot (k\nabla T) + \nabla \cdot \left(\int_0^\infty \frac{4\pi}{3\kappa}\frac{\partial I_{\text{B}}}{\partial T} \, dv\right)\nabla T + Q.$$

SP_1 *approximation*:

$$-\varepsilon^2\nabla \cdot \frac{1}{3\kappa}\nabla\phi + \kappa\phi = 4\pi\kappa I_{\text{B}}$$

$$\rho c_p \left(\frac{\partial}{\partial t}T + \vec{u} \cdot \nabla T\right) = \nabla \cdot (k\nabla T) + \int_0^\infty \nabla \cdot \frac{1}{3\kappa}\nabla\phi \, dv + Q.$$

SP_2 *approximation*:

$$-\varepsilon^2\nabla \cdot \tfrac{1}{3\kappa}\nabla(\phi + \tfrac{4}{5}(\phi - 4\pi I_{\text{B}})) + \kappa\phi = 4\pi\kappa I_{\text{B}},$$

$$\rho c_p \left(\frac{\partial}{\partial t}T + \vec{u} \cdot \nabla T\right) = \nabla \cdot (k\nabla T) + \int_0^\infty \nabla \cdot \frac{1}{3\kappa}\nabla\left(\phi + \frac{4}{5}(\phi - 4\pi I_{\text{B}})\right) dv + Q.$$

SP_3 approximation:

$$-\varepsilon^2 \nabla \cdot \frac{1}{3\kappa} \nabla(\phi + 2\phi_2) + \kappa\phi = 4\pi\kappa I_B,$$

$$-\varepsilon^2 \nabla \cdot \frac{9}{35\kappa} \nabla\phi_2 + \kappa\phi_2 - \frac{2}{5}\kappa\phi = -\frac{8}{5}\pi\kappa I_B,$$

$$\rho c_p \left(\frac{\partial}{\partial t} T + \vec{u} \cdot \nabla T\right) = \nabla \cdot (k\nabla T) + \int_0^\infty \nabla \cdot \frac{1}{3\kappa} \nabla(\phi + 2\phi_2) \, dv + Q.$$

The SP_N approximations can be used to model heat transfer in semitransparent materials. In addition to the equations appropriate boundary conditions have to be stated. For transparent or semitransparent boundaries Marshak's boundary condition can be used to derive appropriate conditions for ϕ and ϕ_2, see [13].

2.4.2. Surface radiation

In the optically thin regime, where the absorption coefficient κ is small, radiative effects can be neglected. If the media is assumed to be not participating, radiation is only relevant between surfaces. Assuming the surfaces to be grey and to be diffuse emitters the radiative heat transfer problem reduces to an integral equation on the surface, e.g., [18]. By formally integrating the radiative heat transfer equation along the direction of travel and taking account of an energy balance at the surface an equation for the radiosity on the surface can be derived. The surface emissive power is proportional to the corresponding value of a black body and can be described by the Stefan–Bolzmann law

$$q_{em} = \kappa\sigma T^4. \tag{21}$$

Here we assume that the emissivity is independent of the wavelength of the emitted radiation. On the other hand points at the surface are also effected by waves emitted or reflected from other points on the surface. The incident heat flux can either penetrate the body or be reflected. We assume the surface to be opaque, which means that the non-reflected waves are totally absorbed and transformed into internal energy in the body. Kirchhoff's law states that the ratio between the absorbed and incident heat fluxes must exactly equal the surface emissivity. The radiosity, the total outgoing heat flux, is the sum of the surface emissive power and the reflected irradiation

$$q_{total} = \kappa\sigma T^4 + (1 - \kappa)q_{in}. \tag{22}$$

The incident heat flux q_{in} is the sum of the contributions of the outgoing fluxes q_{total} from all other points on the surface. The irradiation on the surface is proportional to the radiation emitted by the different parts of the surface itself due to

$$q_{in}(\vec{r}) = \int_\Gamma \omega(\vec{r}, \vec{s}) \Xi(\vec{r}, \vec{s}) q_{total}(\vec{s}) \, d\vec{s}, \tag{23}$$

where Γ is the surface we are considering, $\vec{r}, \vec{s} \in \Gamma$ and $\Xi(\vec{r}, \vec{s})$ the visibility factor, which has a value 1 if the points $\vec{r}$ and $\vec{s}$ see each other, otherwise it has the value 0. The view factor $\omega(\vec{r}, \vec{s})$ has the form

$$\omega(\vec{r}, \vec{s}) = \frac{(\vec{n}_r \cdot (\vec{s} - \vec{r}))(\vec{n}_s \cdot (\vec{r} - \vec{s}))}{\pi\|\vec{s} - \vec{r}\|^4}, \tag{24}$$

where $\vec{n}_r$ and $\vec{n}_s$ are the surface normals. If we define an operator

$$K\lambda(\vec{r}) = \int_\Gamma \omega(\vec{r}, \vec{s}) \Xi(\vec{r}, \vec{s}) \lambda(\vec{s}) \, d\vec{s}, \quad \forall \vec{r} \in \Gamma, \tag{25}$$

we can write $q_{in} = K q_{total}$ and from (22) we get

$$q_{total} = (I - (1 - \kappa)K)^{-1} \sigma\kappa T^4. \tag{26}$$

The heat balance at the surface relating the heat flux caused by conduction to the surface q, the radiosity (22) and (26) and the irradiation (23) then becomes
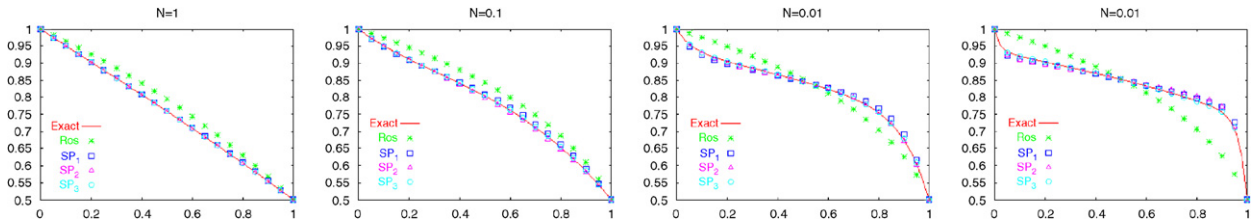
$$q = G(\sigma T^4), \tag{27}$$

Fig. 3. The solution of the exact radiative transfer equation for four different conduction-to-radiation parameters N in comparison with SP_n approximations.

where

$$G = (I - K)(I - (1 - \kappa)K)^{-1}\kappa \tag{28}$$

is the infinite dimensional equivalent of the so-called Gebhart factors. In this form Eq. (27) serves as boundary condition for temperature in all participating components.

2.5. Pseudo-stationary approximation

The specific material system we are interested in allows a simplification of the model. Due to the rather slow solidification the system can be assumed to be in equilibrium at each time step. This allows a pseudo-stationary approximation. Assuming that convection in the melt as well as curvature and undercooling effects at the interface can be neglected the governing equation reduces to

$$-\nabla \cdot k\nabla T + \nabla \vec{i}_{q_r} - \nabla \cdot h\Theta(T - T_{eq}) = Q. \tag{29}$$

The radiative flux $\vec{i}_{q_r}$ is approximated by SP_n models and $\nabla \cdot h\Theta(T - T_{eq})$ describes the heat source due to phase transition, with Θ the phase-function given by $\Theta = 1$ in melt and $\Theta = -1$ in crystal, and h the latent heat per unit area in growth direction given by $h = \rho_{c_0}Lv$, where v is an approximated growth velocity. The equations are coupled through the radiative boundary condition (27). The pseudo-stationary approximation holds when the characteristic time scale of the process, τ_p, is much larger than the characteristic time scale of heat transport in the crystal, τ_h. In VGF growth we assume a uniform thermal gradient in the furnace and the ratio of the time scales are given by [20]

$$\frac{\tau_p}{\tau_h} = \frac{\alpha L}{v B^2}, \tag{30}$$

where α is the thermal diffusivity, L is the length and B is the width of the crystal.

In our case $\alpha = 2 \times 10^{-7}$ s/m², $v < 1$ mm/h and $B = L = 0.2$ m, so $\tau_p/\tau_h \geqslant 4$. The validity of the quasi-steady assumption is additionally checked by numerical experiments analog to [2].

2.5.1. Adaptive finite element approach for SP_3 model with phase change

An adaptive finite element method for the local model of (29), in which only melt and crystal are considered and the boundary conditions at the crucible are given by specified temperatures was introduced by [1] for SP_1 and SP_2. Here we will extend this approach for SP_3.

The diffusion-like structure of the derived equations and boundary conditions allows a variational formulation. We approximate the integrals over the frequency by a sum over frequency bands in which the involved parameters are assumed to be constant. Multiplying with a test function and integrating by parts leads to a weak formulation for the coupled system of equations. These system is discretized by linear finite elements and solved as a system by a Newton method. In order to account for the high spatial resolution needed at the developing boundary layers, an error indicator for temperature is used for local mesh refinement and/or coarsening [3]. The validity of the SP_N method is checked in a one-dimensional test geometry, for which the solution for the full radiative heat transfer equation can be solved, see Fig. 3.
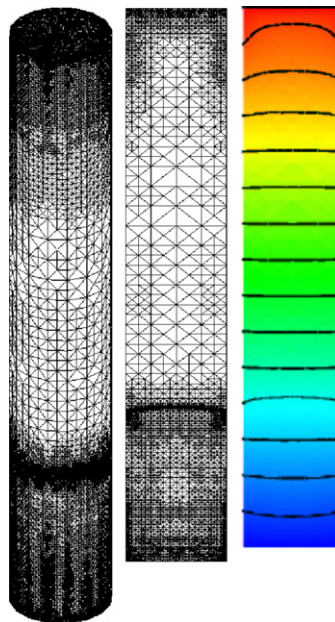
Fig. 4. Adaptive grid, refined at the phase boundary and the developing boundary layers and temperature distributions.
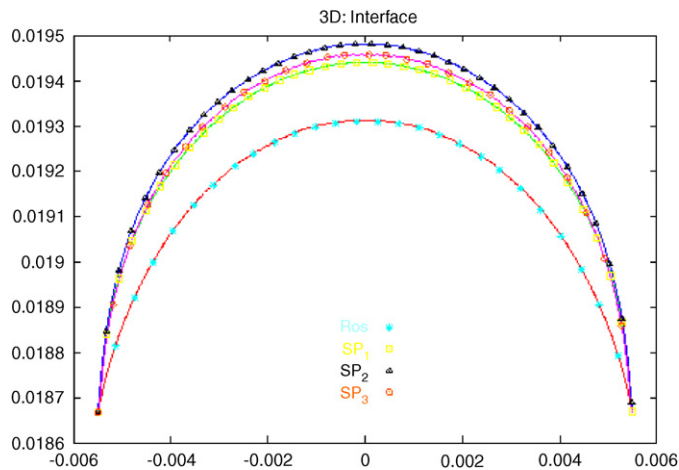

Fig. 5. Interface deflection in center of the cylinder.

The SP$_3$ algorithm is then applied to a full three-dimensional setting. Fig. 4 shows the adaptively refined grid and the temperature field in the crucible. The influence on the phase boundary is shown in Fig. 5. The deviation from the Rosseland approximation is clearly observed.

In conclusion the SP$_N$ equations are a relatively inexpensive way to improve the accuracy of classical diffusion models if compared with the full heat transfer equations.

2.5.2. Adaptive finite element approach for global heat transfer with surface radiation

If internal radiation is neglected an adaptive finite element algorithm for the global model of (29) is described in [22]. Here the volume and surface meshes are decoupled and independently refined according to appropriate error estimates [21].

2.5.3. Numerical approach for two-dimensional rotational symmetric situation

Due to the high computational cost of these three-dimensional models, they are not yet appropriate for efficient process optimization on an industrial scale. For this purpose we therefore restrict ourselves to two-dimensional rotational symmetric situation and a well-established finite volume approximation of (29) in a commercial code. Then, internal radiation can only be modeled by a Rosseland approximation.

3. Process optimization

3.1. Process equation

A single quasi-steady simulation of bulk crystal growth may be symbolized by a furnace equation, F_i. The furnace equation describes the system of coupled nonlinear equations needed to describe the heat and mass transport at a growth stage i of the process:

$$F_i(\vec{T}_i, \vec{p}_i) = 0, \tag{31}$$

where $\vec{T}_i$ is the set of physical unknowns as temperature or velocities, and $\vec{p}_i$ is the parameterized set-up of the process, like geometry, material properties, heating powers, etc. The solution of the furnace equation (31) is the physical state of the growth equipment and the crystal.

The process may then be defined by a sequence of N-steady states. This leads to a process equation:

$$\vec{F}(\vec{T}, \vec{p}) = (F_0(\vec{T}_0, \vec{p}_0), F_1(\vec{T}_1, \vec{p}_1), \ldots, F_N(\vec{T}_N, \vec{p}_N)) = (0, 0 \ldots 0). \tag{32}$$

Often the furnace equations can be treated independently, e.g., $\vec{p}_i$ is known independently of $\vec{p}_j$, $i \neq j$. Then the process equation separates in N independent calculations of a single furnace equation.

An optimization problem can then formally be written as

$$\min_{\vec{p}} \quad f(\vec{p}, \vec{T}(\vec{p})) \tag{33}$$

$$\text{s.t.} \quad \vec{F}(\vec{T}, \vec{p}) = 0, \tag{34}$$

$$p_{1,\min} \leqslant p_1 \leqslant p_{1,\max}, \tag{35}$$

where f is an appropriate objective function, which measures the deviation of the simulated and wanted physical state $\vec{T}$. The parameter space for a single parameter p_1 may be restricted by maximal and minimal values, e.g., tolerance on the material parameters or maximal and minimal heating power.

3.2. Local optimization

Typical optimization problems, we are interested in, are improving an already established process and adapting a numerical model to an experiment. In both cases a local minimizer near the initial state of the model is searched for. Especially adapting concludes that there are small changes in the modeling parameters due to uncertainties in the material specification. Also process improvement is most likely accepted if the changes to the established process are small. Additionally a numerical process model may only be valid in a proximity of the adapted process. So we decided to use a quasi-Newton approach for optimization [17].[1]

A quadratic approximation, m_k, to the objective function is constructed:

$$m_k(q) = f(p_k) + q g_k + \tfrac{1}{2} q^T B_k q, \tag{36}$$

where p_k is the parameter set at iteration k and $q = p - p_k$. g_k is the partial derivative at p_k with respect to p and B_k an approximation to the Hessian matrix. The Hessian is iteratively approximated by the standard BFGS method

$$B_{k+1} = B_k + \frac{B_k s_k s_k^T B_k}{s_k^T B_k s_k} + \frac{y_k y_k^T}{s_k^T y_k}, \tag{37}$$

---

[1] Global optimization by genetic algorithm is recently added to CrysVUn [11].

where $s_k = p_{k+1} - p_k$ and $y_k = g_{k+1} - g_k$. As we use a closed software package it is only possible to solve the furnace equation to a set of parameters. So the needed partial derivatives of the objective function has to be calculated by finite differences. The quadratic subproblem (36) defines a direction, which is chosen for a one-dimensional minimization. One-dimensional minimization is done by a line search with backtracking [17].

The BFGS method is pragmatically stabilized in two details. If the change in the Hessian becomes small and no local minimum is achieved, the BFGS is restarted at this point. Additionally the line search along the Newton direction is replaced by a line search along a polygon defined by steepest descent until the Cauchy point is reached and from the Cauchy point to the local minimizer of the quadratic subproblem. The Newton direction is defined by the minimum of the quadratic approximation of the objective function:

$$g_k = -B_k q. \tag{38}$$

While Cauchy point is defined as the minimum of (36) along the steepest descent direction of the objective function:

$$q^C = -\frac{\|g_k\|^2}{g_k^T B_k g_k} g_k. \tag{39}$$

In trust region techniques this path is called dogleg [17]. So the algorithm will fall back to a steepest descent minimization, whenever the quadratic model is an insufficient approximation to the objective functional.

Constraints in the parameter space for a single parameter p_l are easily included by a logbarrier function [17]

$$Lb(p_l) = -\mu \cdot (\log(p_l - p_{l,\min}) + \log(p_{l,\max} - p_l)) \tag{40}$$

and added to the objective function. The equality constraint due to the process equation is implicitly taken to calculate the objective function. So the process equation is always exactly fulfilled in every optimization step.

3.3. Framework

Nowadays commercial software packages provide robust and stable algorithms to simulate heat and mass transport in a predefined set-up. User friendly interfaces leads to short developing cycle from a CAD drawing to a simulation model. Also some optimization problems may be solved with these packages. But they often lack for an flexible interface to change set-up and other parameters, that can be automatized. Such an interface is needed to use these simulation tools with external optimization tools or to do extensive parameter studies efficiently. Additionally the process equation consist in a set of calculations which should be treated together.

A framework to the software package CrysVUn was developed to overcome this short comings. This interface has four main tasks:

(1) combine several predefined set-ups to define a process model;
(2) customizable parameter changes of the process model;
(3) solve of the process model;
(4) evaluate the process model.

A set of PERL classes are implemented to define and solve the process equation with CrysVUn. If the process equation may be separated in independent furnace equations, a simple schema is used to solve this independent furnace equations parallel on different PCs. In the same way a set of parameters can be treated simultaneously. This allows for more efficient calculation of the gradients by finite differences. The result of this calculation is the physical state of the process, e.g., some temperatures or positions of phase boundaries are needed to calculate the objective function.

4. Process optimization of BaF_2

The aim of modeling is to achieve a process with constant growth velocity of the crystal. In a gauging experiment the phase boundary of a BaF_2 crystal at the crystal axes was monitored in a typical VGF growth process with moving crucible.
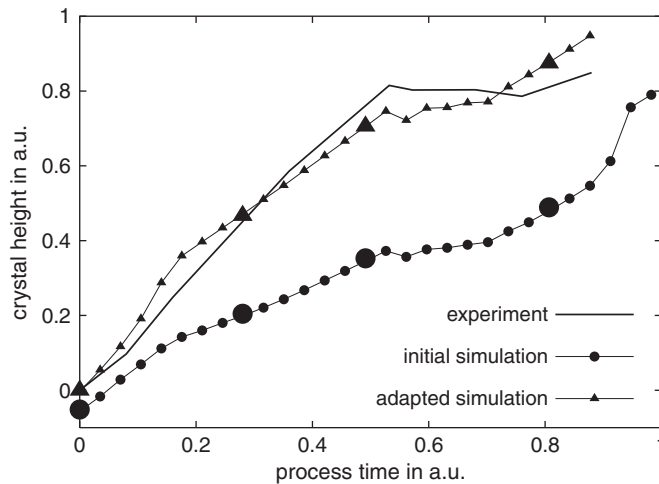
Fig. 6. Position of phase boundary in experiment and simulation. Circles indicate calculation with the initial parameter set. Triangles are phase boundaries obtained after adaption. Big symbols indicate the four snap shots used for adaption of the model.

The process model contains 29 quasi-steady growth stages. The quasi-steady assumption was checked in advance by full time-dependent simulation of a simplified process. The latent heat, respectively, the growth velocity of the crystal, is approximated by experimental measured growth velocity. This allows to decouple process equation and to simulate the different growth stages independently.

In Fig. 6 the result of an initial calculation of the process model and the experiment is shown. The thermal conductivity of the outer isolation has already been roughly adapted to achieve seeding in the simulation model. In order to improve the process the initial process model has to be adapted to provide better agreement with the gauging experiment, a more detailed discussion is given in [4].

4.1. Adaption

For the adaption the process model is reduced to four growth states. Parameters to adapt are the thermal conductivity of outer isolation (p_1), BaF$_2$ crystal (p_2) and crucible support (p_3). Adaption of outer isolation is due to the poor specification of the used graphite felt. This parameter additionally masks uncertainties of the heater powers and overall heat transport to the cooled autoclave. The adaption of the crucible support is meant to model uncertainties of the axial heat transfer to the bottom of the furnace. The crystal is adapted due to the oversimplified model of the semitransparent properties of BaF$_2$. Additionally there is a big uncertainty in the optical properties of BaF$_2$ at high temperatures due to impurities [5,19].

In 5–10 BFGS iteration an improved parameter set can be achieved. During this adaption loop the process equation is solved approximately 40 times. The improved parameter set is $p = (0.089, 1.5, 2.6)$ in which p_1 describes a shift in the thermal conductivity of the outer isolation. p_2 and p_3 are adapting factors to the thermal conductivities of the crucible support and BaF$_2$ crystal, respectively. The large changes in the thermal conductivities of BaF$_2$ and crucible support indicate that this masks some other effects that are not taken into account in the simulation. Nevertheless, pragmatically, this can be taken as a model to predict the phase boundary for this process.

4.2. Optimization

The adapted set of parameters is now used to improve the process. The objective function is now the deviation of the simulated to the ideal position of the phase boundary. Analog to the adaption, the optimization of the process equation separates to 29 independent calculations. The growth velocity is now known by the ideal growth process.

The only available process parameter is the heating power of the lower heater. In Figs. 7 and 8 the results of the optimizations are shown. The ideal position of the phase boundary is achieved at every growth stage, Fig. 7.
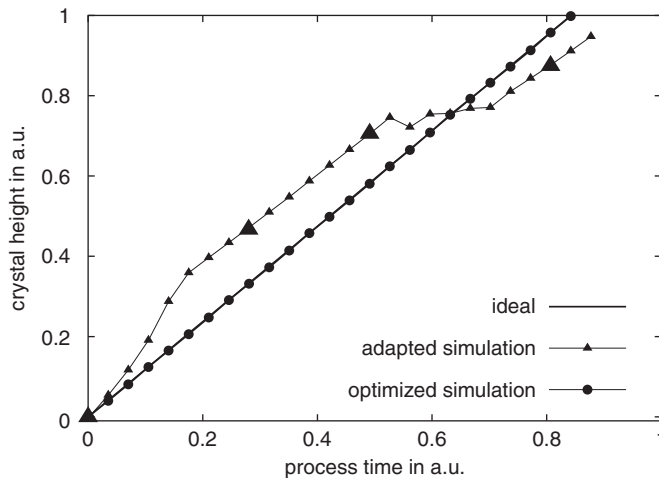
Fig. 7. Position of phase boundary in adapted and optimized model. Triangles are phase boundary obtained after adaption, Fig. 6. Circles are obtained after optimization. The optimized heating power are shown in Fig. 8.
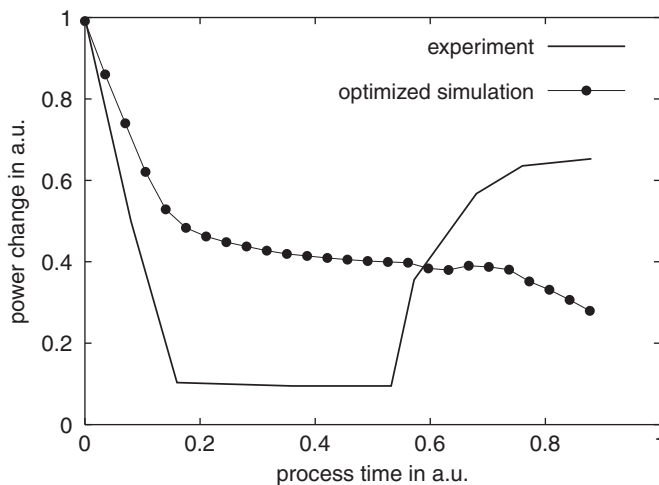

Fig. 8. Heating power in process and predicted after optimization of the adapted model.

An optimized process leads to a smaller decrease of the heating power at the beginning and a smaller increase at the end. Surely, qualitatively this can be easily concluded without any simulation. But the simulation provides a quantitative prediction of the optimized process.

By applying these results to a new growth experiment a new developing cycle can be started. The results of such an experiment will then be used to improve the numerical model to get better predictions.

5. Conclusions

In order to improve crystal growth process, numerical modeling is widely used in industry. To establish an predictive numerical model the global heat transport in the whole furnace has to be considered.

This thermal modeling is described in detail in the first part of the paper. Special emphasis is placed on the modeling of internal radiation. The described SP_N models leads to a set of PDEs, which can be incorporated in established software packages in the future. We applied this model to simple geometrical cases and showed the applicability of the model for crystal growth processes.

The global model of industrial crystal growth processes can be done quite effectively with commercial software packages. In order to use such packages with external optimization algorithms a flexible interface is developed. The interfaces allows to describe complex process models as a set of pseudo-stationary calculations. Changes of parameters and evaluation of the simulation are easily done automatically. This framework is applied to the optimization of a BaF_2 VGF growth. Optimization is done by a modified quasi-Newton method using BFGS updating.

The framework is used to optimize a BaF_2 VGF growth process. In order to get an predictive numerical model some parameters are adapted to a typical growth experiment. In a second step the adapted process model is used to optimize the process.

As industrial demands on simulation results become more and more detailed numerical modeling becomes more and more complex. It is often not possible to develop such software from beginning, which would allow more sophisticated optimization techniques. Additionally the industrial partners request the use of well evaluated and established software packages. Therefore, in order to do efficient process modeling the use of the software should be highly automated, which will allow various optimization tools to be used to solve the engineering problem.

Acknowledgment

References

[1] R. Backofen, T. Bilz, A. Ribalta, A. Voigt, SP_N-approximations of internal radiation in crystal growth of optical materials, J. Crystal Growth 266 (2004) 264–270.
[2] R. Backofen, M. Kurz, G. Müller, Process modeling of the industrial VGF growth process using the software package CrysVUn++, J. Crystal Growth 211 (1–4) (2000) 202–206.
[3] R. Backofen, A. Ribalta, A. Voigt, The influence of internal radiation on the solid–liquid interface in crystal growth of semitransparent materials, in: P. Vincenzi (Ed.), Proc. Computational Modeling and Simulation of Materials, Vol. 44, 2004, pp. 385–392.
[4] R. Backofen, A. Voigt, D. Wulff-Molder, A framework for optimization of crystal growth processes applied to VGF growth of fluorides, J. Crystal Growth 275(1–2) (2005) e349–e353.
[5] F. Barvinschi, O. Bunoiu, I. Nicoara, J. Santailler, T. Duffar, Factors affecting the isotherm shape of semi-transparent BaF_2 crystals grown by bridgman method, J. Crystal Growth 237–239 (2002) 1762–1768.
[6] A. Bates, M. Rothschild, T. Bloomstein, T. Fedynshyn, R.K.V. Liberman, M. Switkes, Review of technology for 157-nm lithography, IBM J. Res. Development 45 (5) (2001) 605–614.
[7] J.H. Burnett, X. Zachary, H. Levine, E.L. Shirley, Intrinsic birefringence in calcium fluoride and barium fluoride, Phys. Rev. B 64 (2001) 241102(R).
[8] CFD Research Corporation, ⟨http://www.cfdrc.com/serv_prod/cfd_multiphysics/software/ace/index.html⟩.
[9] Crystal Growth Laboratory, University Erlangen-Nürnberg, ⟨http://ww6.ww.uni-erlangen.de/cgl/crysvun ⟩ and ⟨http://ww6.ww.uni-erlangen.de/cgl/sthamas⟩.
[10] Fluent Inc.,⟨http://www.fluent.com/software/fidap⟩.
[11] T. Fühner, T. Jung, Use of genetic algorithms for the development and optimization of crystal growth processes, J. Crystal Growth 266 (2004) 229–238.
[12] A.S. Jordana, E.M. Monberga, J.E. Clemansb, Thermal stress theory of dislocation reduction in the vertical gradient freeze (VGF) growth of GaAs and InP, J. Crystal Growth 128 (1–4) (1993) 444–450.
[13] E. Larsen, G. Thömmes, A. Klar, M. Seaid, T. Götz, Simplified P_N approximations to the equations of radiative heat transfer and applications, J. Comput. Phys. 183 (2002) 652–675.
[14] A. Molchanov, U. Hilburger, J. Friedrich, M. Finkbeiner, G. Wehrhan, G. Müller, Experimental verification of the numerical model for a CaF_2 crystal growth process, Crystal Res. Technol. 37 (1) (2002) 77–82.
[15] G. Müller, Experimental analysis and modelling of melt growth processes, J. Crystal Growth 3 (237–239) (2002) 1628–1637.
[16] G. Müller, B. Birkmann, Optimization of VGF-growth of GaAs crystals by the aid of numerical modelling, J. Crystal Growth 237–239 (3) (2002) 1745–1751.
[17] J. Nocedal, S.J. Wright, Numerical Optimization, Springer Series in Operations Research, Springer, New York, 1999.
[18] T. Tiihonen, Stefan–Boltzmann radiation on non-convex surfaces, Math. Meth. Appl. Sci. 20 (1997) 47–57.
[19] G.B. Varlamov, G.N. Vasil'chenko, V.I. Deschko, A.Y. Karvatskii, O.E. Khlebnikov, Thermophysical and optical properties of fluoride crystals and melts, High Temp. High Pressure 21 (1989) 647–656.
[20] A. Virozub, S. Brandon, Revisiting the quasi-steady state approximation for modeling heat transport during directional crystal growth. The growth rate can and should be calculated!, J. Crystal Growth 254 (1–2) (2003) 267–278.
[21] A. Voigt, N. Hanssen, C. Weichmann, The radiosity equation for solving global heat transfer in industrial furnaces, Math. Comput. Model. 39 (2004) 145–150.
[22] A. Voigt, C. Weichmann, Adaptive FEM/BEM coupling for solving global heat transfer in high temperature furnaces, Num. Heat Transfer B, accepted.